PSFC/JA-10-63

Experimental Results on a 1.5 MW, 110 GHz Gyrotron with a Smooth Mirror Mode Converter

Tax, D.S., Choi, E.M., Mastovsky, I., Neilson, J.M.*, Shapiro, M.A., Sirigiri, J.R., Temkin, R.J., Torrezan, A.C.

* Calabazas Creek Research Inc., San Mateo, CA, 94404

2010

Plasma Science and Fusion Center
Massachusetts Institute of Technology
Cambridge MA 02139 USA

This work was supported by the Department of Energy, Office of Fusion Energy Sciences (Grant No. DE-FC02-93ER54186).

Experimental Results on a 1.5 MW, 110 GHz Gyrotron with a Smooth Mirror Mode Converter

D. S. Tax[a], E. M. Choi, I. Mastovsky, J. M. Neilson[b], M. A. Shapiro[a], J. R. Sirigiri, R. J. Temkin, and A. C. Torrezan

[a] Plasma Science and Fusion Center, Massachusetts Institute of Technology, Cambridge, MA, USA 02139

[b] Calabazas Creek Research Inc., San Mateo, CA, USA 94404

Abstract

We present an internal mode converter (IMC) design for a 1.5 MW, 110 GHz gyrotron operating in the $TE_{22,6}$ mode. The launcher, designed using the codes Surf3d and LOT, converts the cavity waveguide mode into a nearly pure Gaussian beam. The Gaussian beam output from the launcher is shaped by a series of 4 smooth, curved mirrors to provide a circular output beam with a flat phase front at the gyrotron window. By employing smooth mirrors rather than mirrors with phase correcting surfaces, such an IMC is less sensitive to alignment issues and can more reliably operate with high efficiency. The IMC performance was verified by both cold test and hot test experiments. Beam pattern measurements in each case were in good agreement with theoretical predictions. The output beam was of high quality with calculations showing that the Gaussian Beam content was 95.8 ± 0.5 % in both hot and cold test.

Introduction

There are very few types of sources capable of efficiently supplying high power in the millimeter wave frequency range. Applications such as electron cyclotron heating and current drive (ECH, ECCD) in nuclear fusion experiments require large amounts of power, on the order of MWs, at frequencies above 100 GHz. For such applications, there is only one source that can meet the requirements: the gyrotron.

The gyrotron is a vacuum electron device that converts the perpendicular energy of an electron beam emitted by a powerful magnetron injection gun (MIG) into microwave power in a rotating TE mode near cutoff of an open resonator cavity in the presence of a static magnetic field. The schematic of MIT's 1.5 MW, 110 GHz gyrotron is shown in Fig. 1. A tunable gun coil at the MIG cathode allows for alteration of the magnetic compression ratio which enables tuning of important electron beam parameters like the ratio of perpendicular to parallel electron velocity α and the beam radius r_b. The beam passes through a smooth cylindrical cavity within the bore of a superconducting magnet where the interaction between the electron beam and the waveguide mode takes place. The walls in the next region of the tube are tapered to optimize the efficiency of the interaction and to increase the wall radius to the optimal size of the internal mode converter (IMC). The microwave power then propagates through the IMC and is

extracted through a window, while the spent electron beam passes through to the collector.

For high power gyrotrons, like those required for plasma heating in nuclear fusion experiments, high efficiency is very important not only to minimize the prime power required for operation, but also to guarantee satisfactory operation over the lifespan of the device. The overall efficiency of the gyrotron is naturally limited by the interaction efficiency between the electron beam and the microwaves; however, in practice, efficiencies will be lower than the theoretical value. This efficiency drop occurs due to a variety of reasons including effects relating to physical principles, such as a secondary after-cavity interaction [1,2], and experimental effects relating to the design and construction of the components, such as the IMC.

The IMC is tasked with converting power from the high order TE mode in the gyrotron cavity into a more useful form, like a Gaussian beam in free space. The IMC consists of a launcher that transforms the cavity mode into a Gaussian beam and a set of mirrors that will direct the power towards the window. The IMC performance can be quantified in a couple of ways. First, there may be excessive lost power in the IMC arising from excessive Ohmic loss in the launcher, from reflection of power back towards the gun, or from losses due to stray radiation, that is power emitted from the launcher which is not intercepted by the surfaces of the mirrors. Another measure of the performance of the IMC is the quality of the output beam, where we define the highest quality beam as an output whose mode content is described by a pure fundamental Gaussian beam with a flat phase front at the window. For ECH applications, the Gaussian beam emitted by the gyrotron will be coupled into large cylindrical corrugated waveguide for transmission to the reactor chamber where it will be used to heat the plasma. The transmission efficiency of the gyrotron power is directly related to the Gaussian beam content of the output beam. For a beam with low Gaussian beam content or one that is highly elliptical, there will be additional loss due to the excitation of higher order modes in the large, overmoded transmission lines connecting the gyrotron and the target reactor [3,4]. In addition, misalignments between the beam and the transmission lines, via tilt or offset, can also result in increased loss, however many systems will implement a matching optics unit (MOU) to eliminate such effects. An MOU could also be implemented with the IMC described in this paper. Recent calculations have shown that about 95 % Gaussian beam content would be required to satisfy ITER's transmission line loss allowance based on the latest designs [5]. The IMC is thus an integral component not just in terms of the efficiency of the gyrotron itself, but also in terms of the gyrotron's effectiveness for its various applications.

In this paper, we discuss the mode converter that was built and installed on a 1.5 MW, 110 GHz gyrotron operating in the $TE_{22,6}$ mode. We present the launcher design by Calabazas Creek Research using the codes Surf3d and LOT [6] as well as the design for a set of four smooth, curved mirrors that shape the elliptical Gaussian beam output of the launcher into a circular beam with a flat phase front at the gyrotron window. The IMC performance was verified by both cold test and hot test experiments, whose results will be discussed.

Mode Converter Design

The gyrotron's internal mode converter (IMC) is comprised of two sections: a launcher where the cavity's TE mode is altered via wall perturbations to emit a Gaussian beam, and a set of mirrors which shape the launched fields to provide a circular output with the correct beam waist at the window. While many IMC designs employ mirrors with phase correcting surfaces to improve the Gaussian content of the beam, the design presented here only uses smooth curved mirrors. Due to the layout of the gyrotron, namely the diameter of the tube and the distance from the launcher tip to the window, a 4 mirror system is required and will consist of 3 smooth curved mirrors and one mirror, mirror 3, that is perfectly flat.

The launcher is a cylindrical waveguide that has a helical cut at the output to launch the microwave power onto the surface of the first mirror [7]. The walls of the launcher are dimpled, generating a mode mixture within the launcher and forming a Gaussian field distribution along the surface of the wall that propagates out according to the helical cut. Though analytical expressions can be used to determine the necessary wall profile, numerical codes are better suited to optimize the launcher design in order to maximize performance. One such code is the Launcher Optimization Tool (LOT), developed by Calabazas Creek Research (CCR). LOT takes a wall deformation of general form:

$$r(\varphi, z) = r_0 + \kappa z + \sum_l \sum_m a_{lm}(z)\cos(H_{lm}(z) - l\varphi) \quad (1)$$

where r_0 is the average wall radius, κ is the tapered slope and the spline points of cubic splines $a_{lm}(z)$ and $H_{lm}(z)$ are the free parameters. A series of modes whose mixture will bunch the fields both longitudinally and azimuthally is then considered. These modes will have equal caustic radii to the $TE_{22,6}$ mode and the longitudinal bunching modes will have interference lengths close to the launcher cut length while the azimuthal bunching modes will have Bessel function zeros similar to the $TE_{22,6}$ mode. The azimuthal bunching modes are thus of the form $TE_{22+/-3,6-/+1}$ and the longitudinal bunching modes are of the form $TE_{22+/-1,6}$. The full set of modes used in the launcher simulations were as follows: $TE_{19\pm1,7}$, $TE_{22\pm1,6}$, $TE_{25\pm1,5}$, $TE_{24,6}$, $TE_{16,8}$, $TE_{17,8}$. The mode mixture that is generated within the launcher due to the wall perturbations is calculated and the optimization process then aims to minimize the field along the helical launcher cut and maximize the Gaussian content at the aperture. To determine the radiated field from the aperture, the code employs a coupled mode theory along with a Stratton-Chu formulation as has been done previously [8]. The improvement in the pre-shaped beams emitted by these latest launchers has greatly helped in improving the overall efficiency of the IMC and the quality of the output beams, and has also allowed for simplifications in the design of the mirror system.

Previously, in order to get output beams with very high Gaussian beam content, many IMCs employed phase correcting surfaces on two of the mirrors, meaning that their surfaces were not simply smooth [9]. Using simulation codes, the field distribution at the first mirror was calculated. Then, knowing that a particular beam waist and field distribution is desired at the window location, a phase retrieval code [10] would be employed to calculate the necessary mirror surfaces to satisfy the transition [11]. While such a method in theory can provide a nearly perfect Gaussian beam output, when considering that the real fields emitted by the launcher may not be identical to the simulated fields and that the alignment of the mirrors will not necessarily be exact, it is

understandable that in practice, the IMC will not perform quite as expected. With more recent launchers designed using the latest codes, phase correcting surfaces on the mirrors are unnecessary. Designing a set of mirrors thus simplifies to applying Gaussian beam optics along with the aid of numerical simulations to determine the focal radii of the smooth mirrors that will focus the beam to the proper waist and proportion at the window.

We now apply these principles to the design of an IMC for a 1.5 MW, 110 GHz gyrotron operating in the $TE_{22,6}$ mode. The gyrotron operates at a voltage of 96 kV with 3 μs pulses and a beam current of 40 A. The main magnetic field is 4.3 T and the α value, the ratio of transverse to axial electron velocity, is 1.4. The IMC design constraints are the input to the launcher, which will be the fields of a $TE_{22,6}$ mode within a waveguide of radius 2.096 cm, and the physical dimensions of the whole system which must fit inside the tube and provide an output beam normal to and centered through the gyrotron window. The launcher wall profile is designed using the LOT code. The designed launcher is 16.4 cm long with a slight uptaper of 0.35º and the profile of the dimpled walls is shown in Fig. 2. The wall perturbations of Fig. 2 generate a mixture of modes within the launcher as the wave propagates down the waveguide which results in the field pattern along the waveguide surface seen in Fig. 3. The launcher geometry is then exported to the code Surf3D for verification of the output beam. Surf3D is a computer code that calculates the rf field scattered from a metal surface by solving the electric field integral equation for an unknown surface current using the method of moments [12,13]. The simulated output calculated by Surf3D along a cylindrical surface at the launcher tip with a radius of 5 cm is shown in Fig. 4. The output beam has high Gaussian content and is without significant sidelobes up to the -30 dB level.

Since the design of the mirrors is based on the output of the launcher, it was important to confirm the theoretically predicted beam pattern with a measurement. A cold test measurement of the launcher output was performed by our collaborators at the University of Wisconsin, R. Vernon and D. Minerath, since they had a readily available scanner system capable of measuring data in cylindrical planes. The result of their measurement is shown in Fig. 5. The agreement between theory and measurement is quite good as the 9 dB beam widths of 2.95 cm along the axis and 60º along the azimuth from the theoretical calculation of Fig. 4 agree well with their respective values from the measurement of 2.9 cm and 70º in Fig. 5. We do note that the sidelobes in the measurement are somewhat larger, reaching the -20 dB level, but are nonetheless still quite small. The small discrepancy between theory and experiment is likely attributed to impurities in the $TE_{22,6}$ mode generator [14] that is necessary to perform these low power tests, however other sources of error such as machining errors in the launcher and misalignments in the measurement system may also play a role [9].

The mirror system is comprised of 4 smooth mirrors. The first two mirrors shape the beam along one axis each, with mirror 1 shaping the beam in the vertical plane (x) and mirror 2 shaping the beam in the axial plane (z). Mirror 3 is perfectly flat and is present only due to the orientation of the gyrotron, while mirror 4 is the only mirror to have curvature along both axes. The layout of the system of mirrors of the IMC is shown in Fig. 6. The mirror system design begins by analyzing the radiated field pattern from the launcher obtained via Surf3D and using it to propagate the fields to the location of mirror 1, a cylindrical surface with a radius of 5 cm around the launcher. The first mirror must also be shifted by the caustic radius due to the way the fields are radiated from the

launcher. The surface of the first mirror is defined by a parabolic cylinder with a focal length of 5 cm and is shifted in the x direction by the caustic radius, 1.06 cm. To determine the incident fields on the second mirror, the numerical code SCATTER is used. SCATTER is a code which computes the radiated field at an arbitrary metal surface using the Stratton-Chu formula [8]. Based on SCATTER simulations and Gaussian beam optics [15,16], mirror 2 is determined to have a regular cylindrical surface with a curvature radius of 62 cm. Finally, SCATTER is used to propagate the fields onto the surface of the flat mirror 3 and then onto the surface of mirror 4 which is oriented in such a way as to propagate the output beam normal to the window. The curvature radii of mirror 4 are calculated to be 104 cm in the axial plane and 209 cm in the azimuthal plane. Table 1 summarizes the location, curvature radii, and physical dimensions of all 4 mirrors and also shows the theoretical beam waists on the surface of each. With the system of mirrors fully defined, the output fields at the window location can then be simulated using SCATTER. The field amplitude is shown in Fig. 7, while the phase distribution along each axis is shown in Fig. 8. The theoretical beam at the window location is circular with beam waists $w_x = w_z \approx 2.9$ cm and the phase front is flat in the region where the field amplitude is within 3 dB of the peak value.

Cold Test Results

To perform the cold test measurements, we used a $TE_{22,6}$ mode generator [14]. The mode generator converts the fundamental mode of rectangular WR-8 waveguide into the $TE_{22,6}$ mode in a cylindrical waveguide with the proper dimensions for the launcher. In order to verify the performance of the IMC, we would like to accurately measure the beam pattern at the window location. For this task, we use a 3-axis scanner along with a measurement system. For the measurements, we opted to use a vector network analyzer (VNA), specifically the Agilent E8363B PNA, along with a set of F band (90-140 GHz) Oleson millimeter-wave heads. The VNA provides for very accurate, repeatable results and if the transmission through the system is sufficiently high then it can provide excellent dynamic range and low SNR. To measure the field patterns, we mounted the receiving head of the VNA to the 3-axis scanner and attached a small cut waveguide antenna, allowing us to sample the fields over a small area. Scanning using this technique is quite fast, and we were thus able to get rather large grids for the data, typically 50 x 50 points, with a resolution of about 3 mm.

While the VNA is capable of measuring both the amplitude and the phase of the radiated fields, we found it more reliable to only rely on the amplitude data. The main reasons for this were the increased sensitivity in the phase measurement to slight misalignments between the scanner and the IMC and increased noise in the phase measurement around the edges of the beam. An alternative approach to obtaining the phase is to measure the amplitude in several planes and then to apply a phase retrieval code to recover the phase values. Since the experimental setup allows for quick measurements in several planes, this approach was logical.

The phase retrieval method is the same that was used on previous mode converter designs where 2 mirrors have phase correcting surfaces [11]. The method involves taking measured amplitude data in at least two planes. An initial phase, a flat phase of 0 for example, is assigned to the first measurement plane. These fields, amplitude and phase,

are then propagated forward to the second measurement plane. At the second plane, we retain the propagated phase values, however the propagated amplitude values are replaced by the experimentally measured amplitudes. This combination of experimental amplitudes and calculated phases are then propagated back to the first plane. A convergence parameter is defined by the difference between the propagated amplitudes and the experimentally measured amplitudes. The process of replacing the propagated amplitudes with the experimentally measured amplitudes and propagating to the other measurement plane is repeated until the convergence criterion is met at which point accurate amplitude and phase data has been recovered. With amplitude and phase values known in a particular plane, the fields at other locations may also be determined.

By measuring the fields directly at the window location, we can quickly verify the size and shape of the beam. Fig. 9 shows the beam pattern measured at the window location along with a marking showing the size of the window itself. Scans of other planes along the axis of the beam showed that the beam is indeed focusing approximately at the location of the window. At the window location, we measured a Gaussian beam waist of w_x = 2.7 cm and w_z = 2.9 cm which compares well to the beam waist of $w_z = w_x$ = 2.9 cm of the theoretical output beam at the window in Fig. 5. We were able to obtain a dynamic range of over 30 dB in such cold test measurements.

As mentioned in the introduction, the Gaussian beam content is an important parameter in determining the resultant loss of the gyrotron power within a transmission line. In order to calculate the Gaussian content of the output beam, we require both amplitude and phase data, and thus perform measurements in several planes and apply the phase retrieval algorithm to extract phase values at the window location. The Gaussian beam content is determined using the following expression:

$$GB\% = \frac{\left| \int A_{Gaussian}(\alpha_x, \alpha_z, W, x, z) A^*_{Experimental}(x, z) dxdz \right|^2}{\int \left| A_{Gaussian}(\alpha_x, \alpha_z, W, x, z) \right|^2 dxdz \int \left| A_{Experimental}(x, z) \right|^2 dxdz}. \qquad (2)$$

where $A_{Experimental}$ is the complex measured fields, $A_{Gaussian}$ is the complex theoretical fields of a round Gaussian beam with beam waist W and tilt angles α_x and α_z, and * represents the complex conjugate. When calculating Gaussian beam content, we allow for a small tilt in the theoretical Gaussian beam by optimizing the *GB*% over the angles α_x and α_z. This is done because a perceived tilt may be present in the phase retrieved Gaussian beam resulting from a small misalignment of the measurement system. This will occur when the scanner is not perfectly parallel to the window and the center of the Gaussian beam will shift from plane to plane. Using this method, we calculated a Gaussian beam content of 95.3 % for a Gaussian beam with W = 2.8 cm. This is very good result as such high quality output beams are required to keep transmission line losses at an acceptable level on projects like ITER.

Hot Test Results

The IMC was installed on a 1.5 MW, 110 GHz pulsed gyrotron operating in the $TE_{22,6}$ mode whose schematic is shown in Fig. 1. The gyrotron utilizes 3 μs pulses with a main magnetic field of 4.3 T and operates nominally at 96 kV and 40 A to produce a power of

1.5 MW. This high-power operating point however is located along the edge of the parameter space where stable excitation of the $TE_{22,6}$ mode occurs and operation can potentially be somewhat unstable over longer periods of time. As a result, for the purposes of this experiment, we elect to operate at the more stable operating point of 98 kV and 43 A with an output power of 1.2 MW. The launcher performance should be identical at this second, more stable operating point.

Just like in the cold test, we would like to obtain accurate field patterns of the Gaussian output beam of the gyrotron. For this experiment, we use a 2-axis scanner and an rf diode to measure the fields. We connect a programmable variable attenuator to the diode and mount it on the scanner. Again, we connect a cut waveguide antenna to measure the fields over a small area as we move it across the measurement plane. At each point, rather than recording the diode signal, we instead choose to record the level of attenuation that results in the same diode signal. This method allows us to eliminate any nonlinear behavior in the diode response and also serves to protect the diode from large signals that would damage it and render it useless. The downside of this approach is that scans take significantly longer to perform than they do when using the VNA in cold test since the attenuation must be ramped down slowly in order to avoid saturating the diode. To further protect the diode, we include a fixed attenuator that ensures the power reaching the diode is not too high at the beam center. Since this measurement technique requires more time than the VNA measurement, data grids were kept smaller, typically using 25 x 25 points and resolutions on the order of 1 cm.

Unlike in cold test, it is impossible to measure the fields directly at the window in the hot test experiment. In fact, it is not advisable to measure right up close near the window either since power can be reflected back into the gyrotron and the power received by the measuring antenna would be unnecessarily high. As a result, it is necessary to apply the phase retrieval method that was described in the previous section. In order to determine the amplitude and phase of the fields at the window, we simply need to measure the amplitudes in several planes far from the gyrotron. For this experiment, we opted to measure the fields along planes located 80, 100, and 120 cm from the gyrotron window. The field pattern measured in the plane 1 m away from the gyrotron window is shown in Fig. 10. Using this measurement technique, we are able to achieve a dynamic range of over 40 dB. Measurements are also highly repeatable with low noise, having error bars of approximately ± 0.3 dB at each point as a result of a slight variation in diode voltage from pulse to pulse as well as the necessity of including a small range of diode voltages that will be deemed constant voltage in order to keep scan times reasonable.

Applying the phase retrieval code to the measured field patterns yields the beam at the window shown in Fig. 11. The beam waists determined from the phase retrieved beam are w_x = 2.9 cm and w_z = 3.0 cm. Table 2 compares the beam waists measured in both hot and cold test with the theoretical beam calculated using SCATTER, and all values are in good agreement. The Gaussian beam content of the phase retrieved fields from the hot test was also analyzed in the same manner as was previously described and was found to be 96.3 % for a Gaussian beam with W = 2.9 cm. This result compares well with the cold test measurement of 95.3 % using a Gaussian beam with W = 2.8 cm. A small difference between the two measurements is to be expected due to some impurities in the mode of the $TE_{22,6}$ mode generator used for cold test, however the agreement is

still quite good. It is also important to note that the hot test beam agreed best for the Gaussian beam of the correct size according to the theoretical prediction, that is $w_x = w_z =$ 2.9 cm.

Conclusions

We have presented the design of a gyrotron internal mode converter (IMC). With improved codes, the pre-shaped beam emitted from the launcher is highly Gaussian, thus the gyrotron mirrors can be smooth, without the need for phase correction on the surface. As a result, this allows the IMC to be less susceptible to alignment errors when installed in the gyrotron and can provide an output beam with very high Gaussian content.

We tested the IMC in both cold test and hot test. The agreement between theoretical expectation and cold test measurement was very good. Hot test measurements were also in good agreement and demonstrated successful operation of the gyrotron with the new mode converter. In experiment, we determined that the Gaussian beam content of the output was 95.8 ± 0.5 %. This is an excellent result as it demonstrates that IMCs with smooth mirrors in high power gyrotrons can achieve the necessary Gaussian beam content required by their applications. The high Gaussian beam content is very important in keeping losses low in the systems that utilize the gyrotron power such as transmission lines for electron cyclotron heating in nuclear fusion experiments.

The measurement techniques presented in this paper are also an improvement over those typically used in such experiments. In both hot and cold test, we were able to measure with a dynamic range of over 30 dB. This allows for very high quality beam pattern measurements which can be effectively used along with a phase retrieval code to obtain amplitude and phase data at the window. By having such accurate measurements, it greatly enhances one's ability to analyze the gyrotron output beam.

Acknowledgements

The authors would like to thank Monica Blank and Philipp Borchard of CPI for the fabrication of the launcher and D. Minerath and R. Vernon of the University of Wisconsin for their work on the launcher cold test. This work was supported by the Department of Energy, Office of Fusion Energy Sciences.

References

1. V. E. Zapevalov and M. A. Moiseev, "Influence of aftercavity interaction on gyrotron efficiency," *Radiophysics And Quantum Electronics*, **47**, 520-527 (2004).

2. E. M. Choi, M. A. Shapiro, J. R. Sirigiri, and R. J. Temkin, "Experimental observation of the effect of aftercavity interaction in a depressed collector gyrotron oscillator," *Physics of Plasmas*, **14**, 093302 (2007).

3. D. S. Tax et al, "Mode conversion losses in ITER transmission lines," *Proc. Of 33rd Intl. Conf. IR, MM and THz Waves*, Sept 2008, 10.1109/ICIMW.2008.4665590 (2008).

4. K. Ohkubo, S. Kubo, H. Idei, M. Sato, T. Shimozuma, and Y. Takita, "Coupling of tilting gaussian beam with hybrid mode in the corrugated waveguide," *Int. J. Infrared Millim. Waves*, **18**(1), 23-41 (1997).

5. M. A. Shapiro, E. J. Kowalski, J. R. Sirigiri, D. S. Tax, R. J. Temkin, T. S. Bigelow, J. B. Caughman, and D. A. Rasmussen, "Loss estimate for ITER ECH transmission line including multimode propagation," *Fusion Science and Technology*, **57**(3), 196-207 (2010).

6. J. M. Neilson, "Optimal synthesis of quasi-optical launchers for high-power gyrotrons," *IEEE Trans. Plasma Science*, **34**, 635-641 (2006).

7. A. A. Bogdashov and G. G. Denisov, "Asymptotic theory of high-efficiency converters of higher-order waveguide modes into eigenwaves of open mirror lines," *Radiophys. & Quantum Electronics*, **47** (4), 283-296 (2004).

8. M. Blank, K. Kreischer, and R. J. Temkin, "Theoretical and experimental investigation of a quasi-optical mode converter for a 110-GHz gyrotron," *IEEE Transactions on Plasma Science*, **24**(3), 1058-1066 (1996).

9. M. P. Perkins, R. Cao, J. M. Neilson, R. J. Vernon, "A high efficiency launcher and mirror system for use in a 110 GHz $TE_{22,6}$ mode gyrotron," *International Journal of Infrared and Millimeter Waves*, **28**(3), 207-218 (2007).

10. A. V. Chirkov, G. G. Denisov, and N. L. Aleksandrov, 3D wavebeam field reconstruction from intensity measurements in a few cross sections," *Optics Communications*, **115**, 449-452 (1995).

11. D. R. Denison, T. S. Chu, M. A. Shapiro, and R. J. Temkin, "Gyrotron internal mode converter reflector shaping from measured field intensity," *IEEE Transactions on Plasma Science*, **27**(2), 512-519 (1999).

12. J. M. Neilson, "Surf3D and TOL: computer codes for design and analysis of high-performance QO launchers in gyrotrons," *29th International Conference on Infrared and Millimeter Waves,* Karlsruhe, Germany, 667-668, Sept. 27 – Oct. 1, 2004.

13. J. M. Neilson and R. Bunger, "Surface integral equation analysis of quasi-optical launchers," *IEEE Transactions on Plasma Science*, **30**(3), 794-799 (2002).

14. C. Moeller, "A coupled cavity whispering gallery mode transducer," *Conf. Digest 17th Int. Conf. on Infrared and Millimeter Waves*, Pasadena, CA, M3.7 (Dec. 1992).

15. P. F. Goldsmith, *Quasioptical Systems: Gaussian Beam Quasioptical Propagation and Applications*, Wiley Publisher, 1998.

16. D. H. Martin and J. W. Bowen, "Long-wave optics," *IEEE Transactions on Microwave Theory and Techniques*, **41**(10), 1676-1690 (1993).

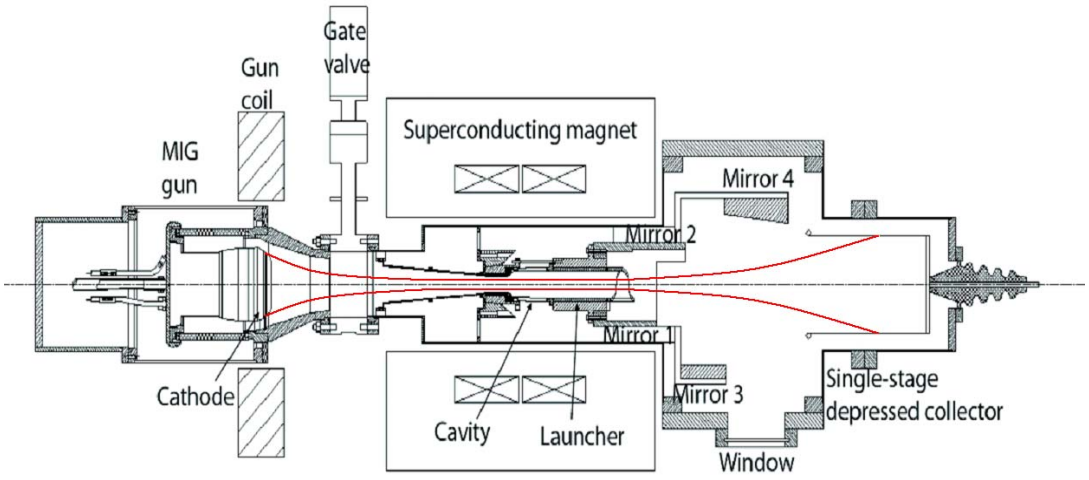

Fig. 1 Schematic of MIT 1.5 MW, 110 GHz gyrotron with an internal mode converter. Annular electron beam is shown in red.

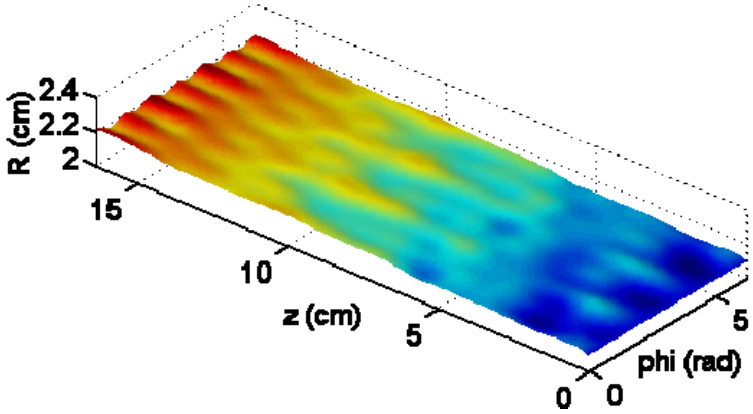

Fig. 2 Optimized wall profile for the launcher calculated by the code LOT. The dimples along the surface of the wall shape the microwave fields within the launcher, generating the field intensities along the wall shown in Fig. 3.

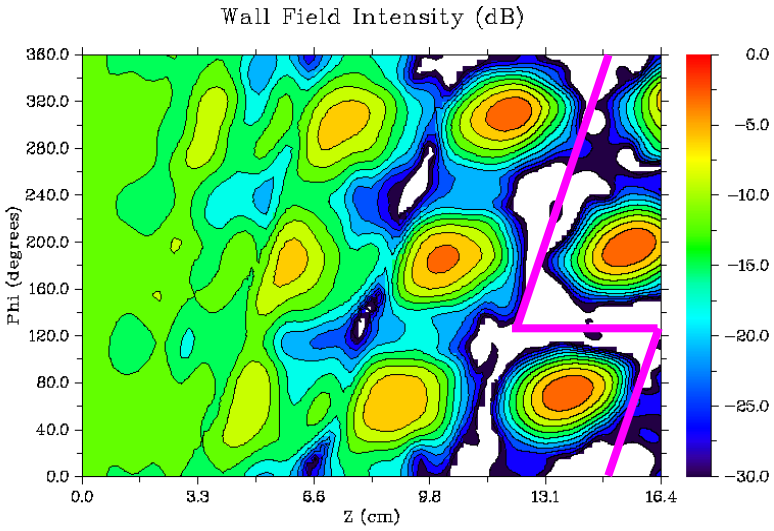

Fig. 3 Field intensity along the wall of the launcher. Left side shows the launcher input where the waveguide is unperturbed while the right side shows the launcher cut.

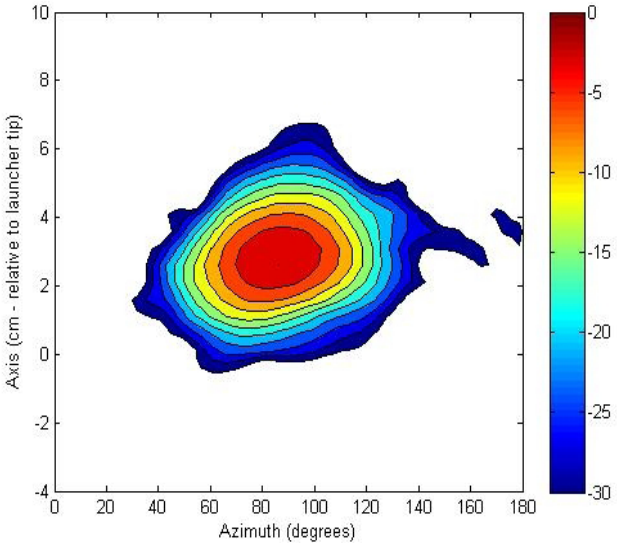

Fig. 4 Surf3D calculation of the output beam of the launcher along a cylinder of r = 5 cm.

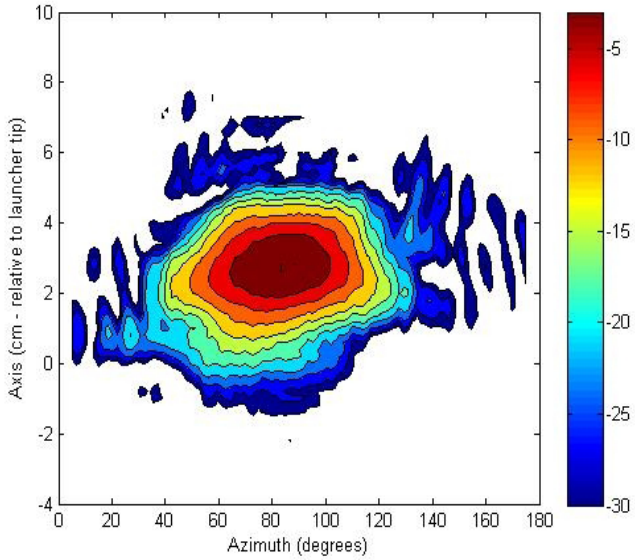

Fig. 5 Cold test of the launcher output measured along a cylinder with r = 5 cm.

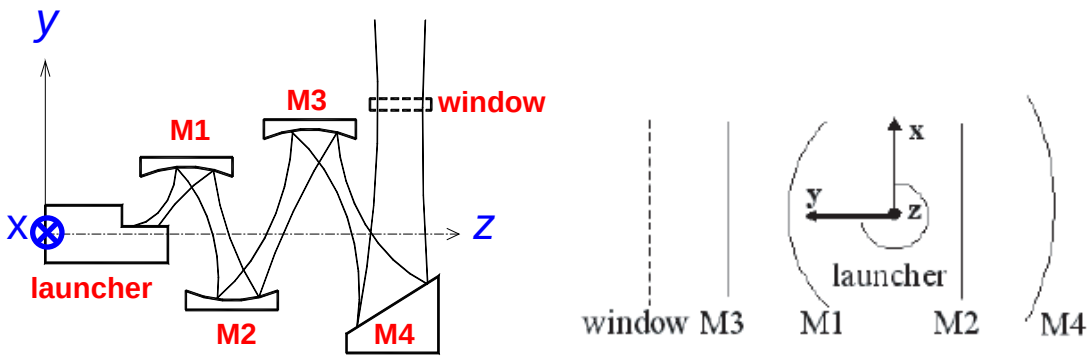

Fig. 6 Layout of the IMC mirror system. Left: side view, Right: axial view

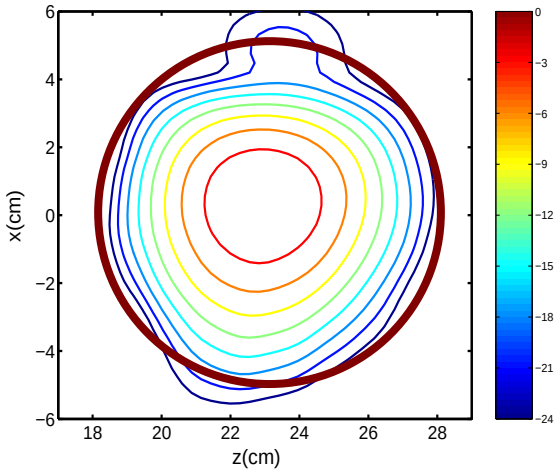

Fig. 7 Theoretical field pattern of the output beam at the window location.

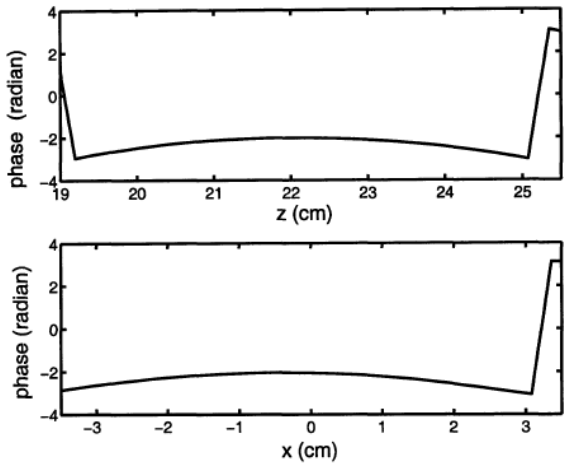

Fig. 8 Phase of the output beam at the window location along each axis.

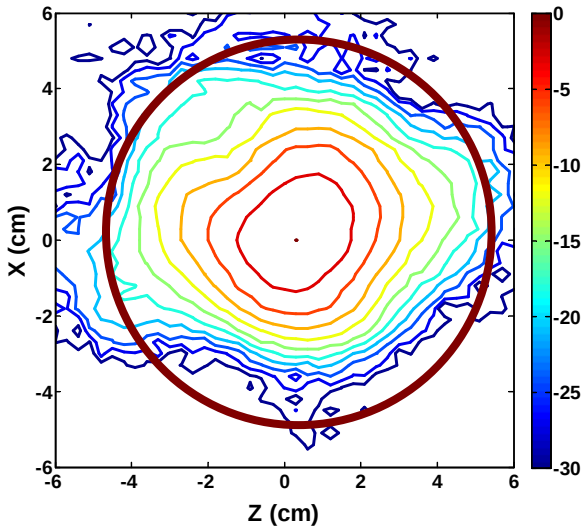

Fig. 9 Cold test measurement of the output beam at the window location.

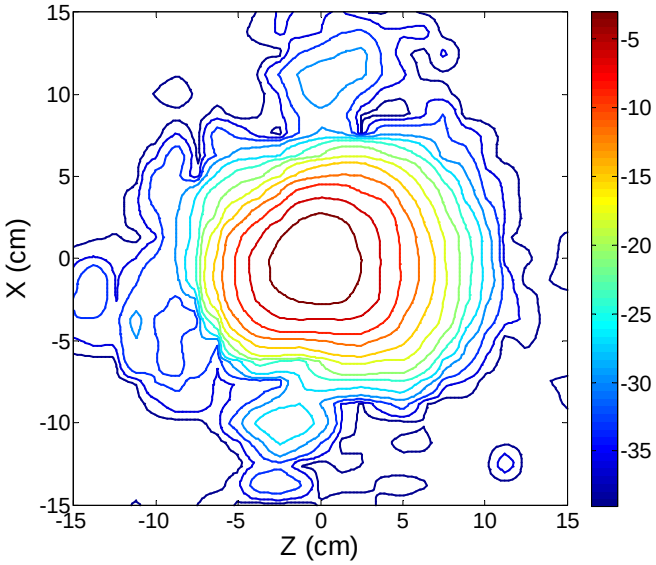

Fig. 10 Beam pattern measured in hot test 1 m from the gyrotron window

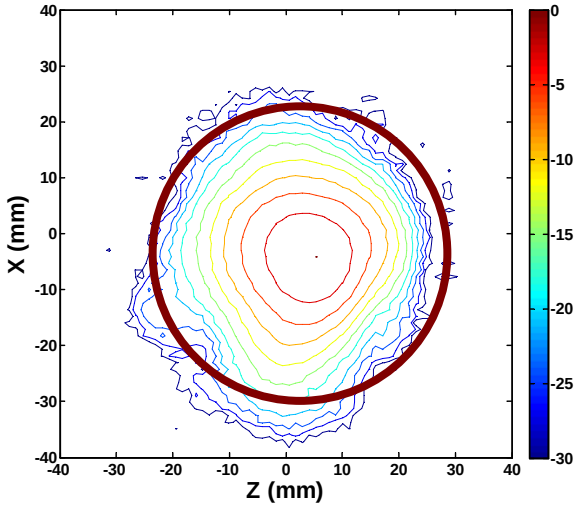

Fig. 11 Calculated output beam using the phase retrieval method based on measured amplitudes in several planes far from the gyrotron.

	Beam size (W_x,W_z) [cm]	Mirror Center (x_m,y_m,z_m) [cm]	Mirror size (d_x,d_z) [cm]	Curvature R_x	Curvature R_z
M1	(2.2,1.13)	(1.059,5,0)	(10,5)	10 cm	Flat
M2	(2.53,1.69)	(0,-5,5.038)	(10.2,6.8)	Flat	62 cm
M3	(2.71,2.474)	(0,11,12.48)	(10.9,10)	Flat	Flat
M4	(3.11,3.11)	(0,-10,22.55)	(14,14)	209 cm	104 cm
Window	(2.93,2.93)	(0,25.4,22.55)	(9.754,9.754)	Flat	Flat

Table 1 IMC mirror system specifications.

Gaussian Beam Waists		
	w_x (cm)	w_z (cm)
Calculation	2.9	2.9
Cold Test	2.7	2.9
Hot Test	2.9	3.0

Table 2 Comparison of beam waists measured experimentally with theoretically calculated values.